Research article

Xiaoping Huang, Kai Chen, Mingxi Qi, Peifeng Zhang, Yu Li, Stephan Winnerl, Harald Schneider, Yuanjie Yang* and Shuang Zhang*

Plasmonic field guided patterning of ordered colloidal nanostructures

https://doi.org/10.1515/nanoph-2018-0211
Received December 2, 2018; revised February 7, 2019; accepted February 8, 2019

Abstract: Nano-patterned colloidal plasmonic metasurfaces are capable of manipulation of light at the subwavelength scale. However, achieving controllable lithography-free nano-patterning for colloidal metasurfaces still remains a major challenge, limiting their full potential in building advanced plasmonic devices. Here, we demonstrate plasmonic field guided patterning (PFGP) of ordered colloidal metallic nano-patterns using orthogonal laser standing evanescent wave (LSEW) fields. We achieved colloidal silver nano-patterns with a large area of 30 mm^2 in <10 min by using orthogonal LSEW fields with a non-focused ultralow fluence irradiation of 0.25 W cm^{-2}. The underlying mechanism of the formation of the nano-patterns is the light-induced polarization of the nanoparticles (NPs), which leads to a dipole-dipole interaction for stabilizing the nano-pattern formation, as confirmed by polarization-dependent surface-enhanced Raman spectroscopy. This optical field-directed self-assembly of NPs opens an avenue for designing and fabricating reconfigurable colloidal nano-patterned metasurfaces in large areas.

Keywords: ordered colloidal nanostructures; plasmonic field guided patterning; polarization stabilizing.

1 Introduction

Plasmonic metasurfaces are metallic patterned subwavelength arrays exhibiting unique macroscopic electromagnetic properties due to the collective response of the individual nanostructures [1–4]. Plasmonic metasurfaces [5–8] are capable of manipulating the phase, amplitude [9], and polarization [10] of light on the subwavelength scale, which may have many applications in advanced photonic devices. Thus far, most plasmonic metasurfaces are fabricated using expensive and time-consuming top-down techniques, such as electron beam lithography and focused ion beam lithography, which set a severe constraint to their practical applications. Meanwhile, bottom-up approaches, such as colloidal metasurfaces, are promising for mass production. They can be designed to display interesting and tunable optical functionalities by tuning the in-plane [11] or out-plane [12] electromagnetic coupling through changing the size, shape of the individual nanoparticles (NPs), and their assemblies [13]. Thus far, there are several methods for fabricating colloidal metasurfaces, such as self-assembly [14], optical printing [15], and optical binding [16], with each method having specific advantages and disadvantages. Self-assembly is a scalable, robust, and tunable method [14]; however, the presence of assembly defects and the typical poor reproducibility limit the uniformity and bandwidth of metasurface performance [17]. Optical printing by focused laser beams can fabricate ordered colloidal arrays with NPs in solution [15]; however, the accuracy and stability of fabrication are influenced by photothermal effects, which hinder the fabrication of complex nanostructured colloidal patterns. Comparing with optical trapping [18–20], optical binding [16] can improve the spatiotemporal stability of

***Corresponding authors: Yuanjie Yang,** School of Physics, University of Electronic Science and Technology of China, Chengdu 610054, China; and Department of Electrical and Computer Engineering, National University of Singapore, Singapore 117583, Singapore, e-mail: dr.yang2003@uestc.edu.cn; and **Shuang Zhang,** School of Physics and Astronomy, University of Birmingham, Birmingham B15 2TT, UK, e-mail: s.zhang@bham.ac.uk
Xiaoping Huang: School of Physics, University of Electronic Science and Technology of China, Chengdu 610054, China; and Institute of Ion Beam Physics and Materials Research, Helmholtz-Zentrum Dresden-Rossendorf, Bautzner Landstraße 400, 01328 Dresden, Germany. https://orcid.org/0000-0002-1996-9335
Kai Chen, Mingxi Qi, Peifeng Zhang and Yu Li: School of Physics, University of Electronic Science and Technology of China, Chengdu 610054, China
Stephan Winnerl and Harald Schneider: Institute of Ion Beam Physics and Materials Research, Helmholtz-Zentrum Dresden-Rossendorf, Bautzner Landstraße 400, 01328 Dresden, Germany

the bound colloidal arrays through enhancing the light intensity of the laser beam. Furthermore, a hybrid method was proposed to fabricate solid nano-patterned plasmonic metasurfaces; however, this method is highly complicated as it involves both top-down lithographic techniques and bottom-up self-assembly [11, 21–23]. Therefore, fabrication of solid nano-patterned colloidal metasurfaces of large areas via a simple and controllable process is highly desirable. Optically mediated interaction between assembled NPs in laser standing waves can cause optical forces and dramatically influence the way they assemble themselves [24–26], enabling to stabilize the near- and far-field interaction among the NPs during the assembly process. This may enlighten a way for trapping and assembling a large number of NPs to solid nano-patterns with a large area.

In this work, we propose and demonstrate plasmonic field guided patterning (PFGP) as a rapid fabrication route for creating large-area nano-patterned colloidal structures, by utilizing orthogonal laser standing evanescent wave (LSEW) fields. The combination of three-dimensional (3D) confined optical tweezers array and ultra-strong optical binding between NPs facilitates assembly of solid nano-patterns on a large scale. Moreover, the 3D optical potential well array induced by the orthogonal (LSEW) fields leads to the stable trapping of NPs. To reduce the photothermal effect, we use a flat-top laser beam with a lower power density (0.25 W cm^{-2}) and specific wavelength (532 nm), deviated but still close to the plasmon resonance wavelength of colloidal Ag NPs (~500 nm). Thus, the cooperative dynamic interplay between the optical driving force and the near-field binding force on the colloidal silver NPs leads to directed assembly of solid nano-patterned metasurfaces in the surface-enhanced orthogonal LSEW fields. Using PFGP, we are able to fabricate diverse colloidal metallic metasurfaces consisting of ordered nano-patterns over a large area of 30 mm^2 via tuning the interference patterns. This PFGP system not only provides a lithography-free and versatile nano-fabrication platform for obtaining metasurfaces with highly hierarchical structures from nanometer to macroscopic scale, but also allows for localized, quantitative investigation of the complex dynamic interaction of polarized colloidal metallic NPs.

2 Results and discussion

2.1 Plasmonic field guided patterning

The ordered colloidal silver nano-patterns are fabricated using the PFGP method. The optical setup of PFGP is illustrated in Figure 1A. The orthogonal LSEW optical fields are constructed at the suspension-glass interface with four *s*-polarized synchronous laser beams of diameter ~5 mm, as shown in Figure 1B. Four collimated flat-top beams are incident normally onto the lateral sides of the quad-frustum prism, and reach the top surface at the same angle with $\theta > \theta_c = \arcsin(n_2/n_1)$, satisfying the total internal reflection at the border between prism and suspension. In this case, four evanescent waves emerge on the prism surface with a propagating wave vector of $k_{tx} = k_0 n_1 \sin\theta$ and a decaying constant of $k_{tz} = jk_0 n_2 \sqrt{n_1^2 \sin\theta / n_2^2 - 1}$ in the direction normal to the interface, leading to formation of LSEW [27–29]. By superimposing the four laser beams together, the orthogonal LSEW fields $\mathbf{E}_{ts}^{2D}$ can be constructed at the prism surface [see Eqs. (S2) and (S3) in Supplementary Information I]. These LSEW fields are given by

$$\mathbf{E}_{ts}^{2D} = -2Ae^{jk_{tz}z}(je^{-j\delta^s})[\gamma \sin(k_{tx}y)\mathbf{e}_x + \sin(k_{tx}x)\mathbf{e}_y], \quad (1)$$

where the time dependence factor is omitted, $A = 2E_{is}\cos\theta/\cos\theta_c$ is the electric field of the evanescent wave with a *s*-polarized incident plain wave E_{is}, $\delta^s = \arctan\left(\sqrt{\sin^2\theta - n_{21}^2}/n_{21}^2\cos\theta\right)$ is the phase change angle at the interface, and γ is the optical power intensity tuning factor, which denotes the electric field amplitude ratio along *x*- and *y*-axis. The combination of field enhancement and confinement in the orthogonal LSEW fields plays a very important role for the formation of NP PFGP on the prism surface [27–29].

The colloidal silver metasurfaces with ordered nano-patterns were fabricated using the PFGP method in the orthogonal LSEW fields. The as-prepared silver colloidal suspension was injected into the enclosed cell on the top surface of a quad-frustum prism. As four laser beams with equal power intensity of 0.25 W cm^{-2} impinge normally onto the four lateral sides of the prism at an angle of 50° (slightly larger than the critical angle), the orthogonal LSEW fields were constructed on the surface of the prism. After irradiation of a few minutes, the colloidal silver metasurface was developed on the prism surface. The size of the metasurface was determined by the laser illumination area and could reach >30 mm^2. Figure 1C shows a typical robust square array of silver NP-based nano-mounds. The nano-mound array extends along the two polarization directions. Especially, the magnified scanning electron microscopy (SEM) image shows that the pattern has a uniform period of 180 nm, which exactly fits with that calculated based on the incident

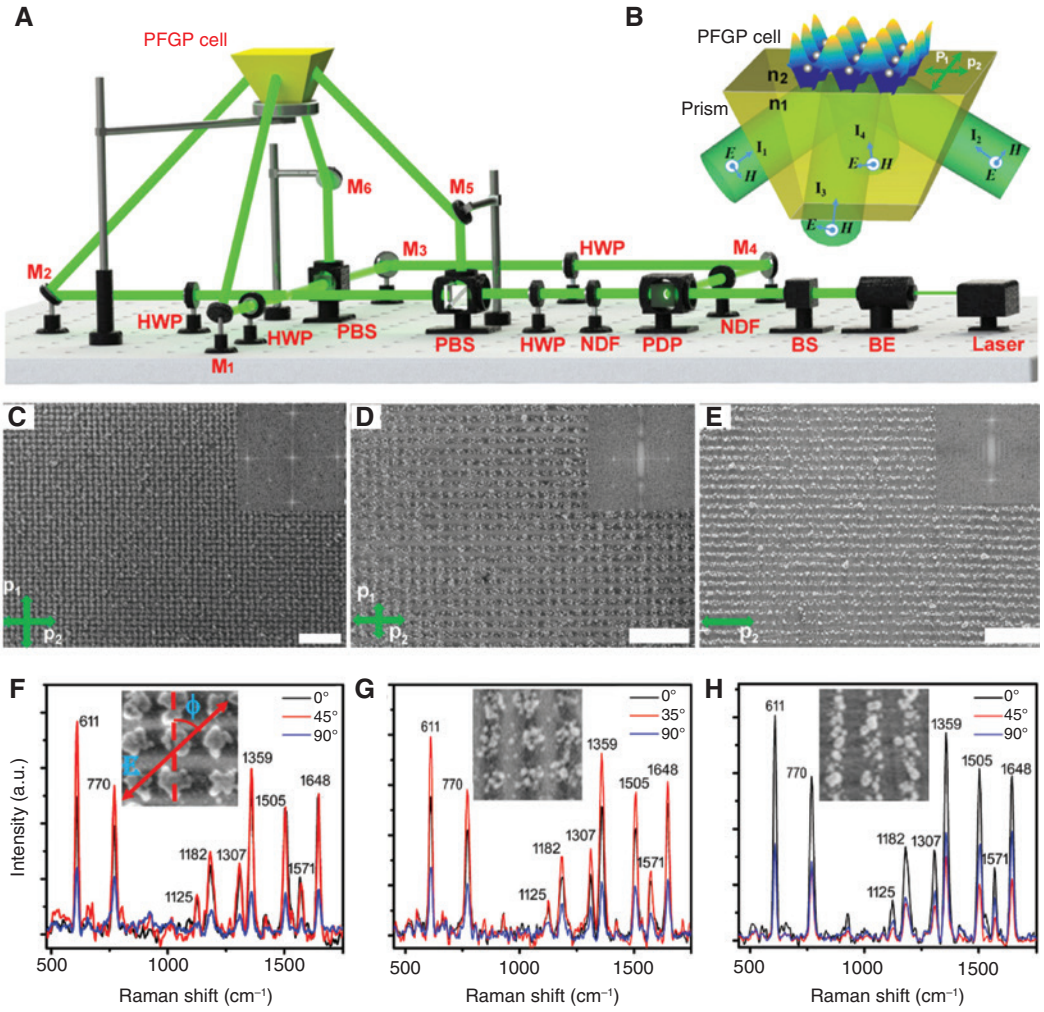

Figure 1: Illustration of the optical setup for PFGP and the SEM images of the patterned colloidal silver nanostructures with anisotropic spectral responses.

(A) The optical setup for PFGP. The light source is an SLM DPSS laser. The optical components of beam expander (BE), power dividing prism (PDP), polarizing beam splitters (PBS), half wave plates (HWP), and neutral density filters (NDF) are used to tune the power and polarizations of the laser beams. A quad-frustum prism enclosed with a glass spacer and a coverslip is used as the PFGP cell. (B) The optical potential array created by orthogonal LSEW fields in the PFGP cell. (C–E) SEM images of the patterned colloidal silver nanostructures fabricated in orthogonal LSEW illumination with power density ratio of 0.25 W cm^{-2} to 0.25 W cm^{-2}, 0.25 W cm^{-2} to 0.125 W cm^{-2}, and single LSEW illumination with power density of 0.25 W cm^{-2}, respectively. The arrows $\vec{p}_1$ and $\vec{p}_2$ denote the polarization of the LSEW. The scale bar in (C)–(E) is 1.0 μm. The insets in (C)–(E) are the FFT maps of the corresponding nano-patterns. (F–H) The p-SERS spectra of rhodamine 6G adsorbed on different patterned colloidal silver nanostructures.

laser wavelength, incident angle, and the glass refractive index. The size of the nano-mounds is tens of nanometers, and the coverage can be tailored flexibly by the laser intensity, irradiation time, and the concentration of silver colloids. Moreover, the fast Fourier transformation (FFT) pattern in the inset of Figure 1C shows a very regular square array structure of the nanostructured pattern. By varying the relative optical intensities of the two orthogonal pairs of beams, in-plane anisotropy of the pattern can be realized. As shown in Figure 1D, when the intensity of one pair of beam is reduced to 0.125 mW, the periodic modulation of the pattern along the corresponding direction is weakened, as shown by the FFT pattern in the inset. Further reducing the intensity of the same pair of beam to zero leads to the formation of a 1D nanowire array pattern, as shown in Figure 1E. To further look into the anisotropic spectral response of the patterned colloidal silver nanostructures, the morphology correlation of polarization-dependent surface-enhanced Raman spectroscopy (p-SERS) was characterized in three major directions, as shown in Figure 1F–H. As shown in Figure 1F, the maximum SERS signal intensities were collected at $\phi = 45°$, whereas much weaker Raman signals were detected for the 0° and 90° polarization

directions (see Supplementary Information II). Meanwhile, Figure 1G,H shows that the maximum SERS signal intensities were obtained at $\phi = 35°$ and 0°, respectively, for the transitional formation of colloidal silver nano-patterns. Therefore, the anisotropic structures in the colloidal metallic nano-patterns leads to the anisotropic electromagnetic enhancement of the SERS signal [30]. Moreover, the scattering spots and the corresponding colored rainbow belt diffracted by the nanostructured silver gratings show good anisotropic optical responses (see Supplementary Information III).

2.2 Analysis of optical forces

The ordered colloidal nanostructures are formed by the directed self-assembly of NPs with the combining exertions of optical forces. To study the cooperative optical forces acting on the colloidal metallic NPs (radius $a \ll \lambda$) in orthogonal LSEW fields $\vec{E}_{ts}^{2D}$, we divide the total optical force into optical gradient force and binding force [26]. The optical gradient force acts on individual NPs placed in an incident field with intensity gradient, and the binding force arises between the NPs mediated by the plasmonic field [26, 31–33]. The time-averaged optical gradient force acting on a colloidal silver NP can be approximated as follows [see Supplementary Eq. (S12)]:

$$\begin{aligned}\mathbf{F}_g = &\frac{4\alpha' \cdot e^{2jk_{tx}z} \cdot \mathrm{E}_{is}^2 \cos^2\theta}{\cos^2\theta_c}\Big\{k_{tx}[\sin(2k_{tx}x) \\ &+ 2\cos(k_{tx}x)\sin(k_{ty}y)]\mathbf{e}_x + \gamma^2 k_{tx}[\sin(2k_{tx}x) \\ &+ 2\cos(k_{ty}y)\sin(k_{tx}x)]\mathbf{e}_y\Big\} + \frac{\alpha' jk_{tz}z}{2}\left|\vec{\mathrm{E}}_{ts}^{2D}\right|^2 \mathbf{e}_z, \end{aligned} \quad (2)$$

where E_{is} is the electric filed component of the s-polarized incident plain wave, and k_{tx} and k_{tz} are the wave vectors of the orthogonal LSEW fields. As both dipoles in the two neighboring particles orient along their relative displacement vector $\mathbf{r}$, the local electric field $\mathbf{E}_{ts}^{2D}$ is parallel to the same direction with the maximum optical binding force given by [26]

$$\mathbf{F}_b = -\frac{3|\alpha|^2}{4\pi\varepsilon_0\varepsilon_m r^4}\left|\vec{\mathrm{E}}_{ts}^{2D}\right|^2 \mathbf{e}_r, \quad (3)$$

where the objects are taken to be identical isotropic polarized spherical NPs.

Based on Eqs. (1) and (2), the maximum optical force versus the beam power density, for a fixed spot size of the incident beam at 5 mm, can be obtained in Figure 2A. More specifically, we achieve a very strong optical gradient force on a 20-nm silver NP at the incident power density of 0.25 W cm^{-2}, which is much stronger than the values for focused Gaussian beam trapping and plasmonic trapping [20, 34] at the same optical power density. This means that our PFGP provides strong enough optical gradient force with the ultralow irradiation of 0.25 W cm^{-2}. At the near-field zone, we can use Eq. (3) to calculate the binding force strength on the assembly of the square array of nano-patterned metasurface, which is shown in Figure 2A. It is observed that the dipolar binding forces increase with decreasing separation between the two silver NPs. In comparison, when the NP separation is near 0.1 nm, the induced dipolar binding force is 10 times higher than the optical gradient force. For much larger NP separation, e.g. 20.0 nm, the dipolar binding force is about the same as the maximum gradient optical force. As such, for very small NP separation (<20.0 nm), the near-field dipole-dipole

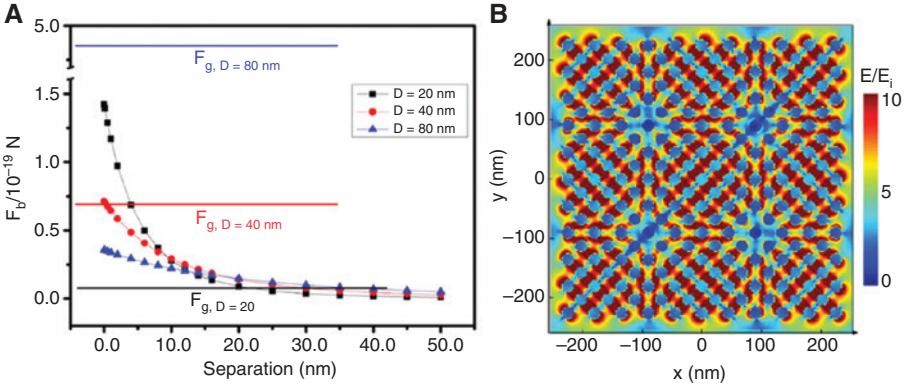

Figure 2: Optical force calculations and dipolar coupling in the orthogonal LSEW fields.
(A) Optical forces exerted on the colloidal silver NPs with different diameters at an illuminating laser intensity of 0.25 W cm^{-2}.
(B) Dipole-dipole coupling pattern of the polarized NPs in the orthogonal LSEW fields.

binding force dominates the assembly mechanism (see Supplementary Figure S2). The dipole-dipole coupling of the polarized silver NPs in the orthogonal LSEW fields can be visualized through simulation, as shown in Figure 2B. The simulated result shows very strong coupling at the hot-spot area, whereas the coupling gets gradually weaker when the NPs approach the darker regions. This periodic modulation of the binding force leads to the formation of a square array of nano-patterned metasurface observed in the experiment.

To obtain a deeper understanding of PFGP for the nano-patterned metasurfaces, the distribution of the optical gradient forces exerted on the colloidal silver NPs in the orthogonal LSEW fields is further investigated in simulation. Figure 3A shows a periodic distribution of the calculated orthogonal LSEW fields when $\gamma = 1$, which form a square lattice array (see Supplementary Figure S3). The spatial distribution of the instantaneous electric field vectors of orthogonal LSEW fields is shown in Figure 3B. As a result of dipolar interaction between the colloidal silver NPs in the orthogonal LSEW fields, a local optical intensity gradient is formed, and the NPs tend to be attracted toward the high field area of the anti-nodes. Figure 3C illustrates the total optical gradient force exerted on NPs in the orthogonal LSEWs. The distribution, magnitude, and direction of the force vectors determine the motion tendency of the colloidal NPs, which shows strong dependence on the spatial distribution of the orthogonal LSEW fields (see Figure S3). Interestingly, from Eq. (1), the z-component of the optical gradient force (last term on the right hand side) proportional to $|E_{is}|^2$ is directed toward the prism surface because of the pure imaginary index k_{tz}. As a result, the z-component of the optical gradient force together with the lateral optical gradient force is responsible for the directed motion and assembly of the colloidal NPs on the prism surface. As for the asymmetric

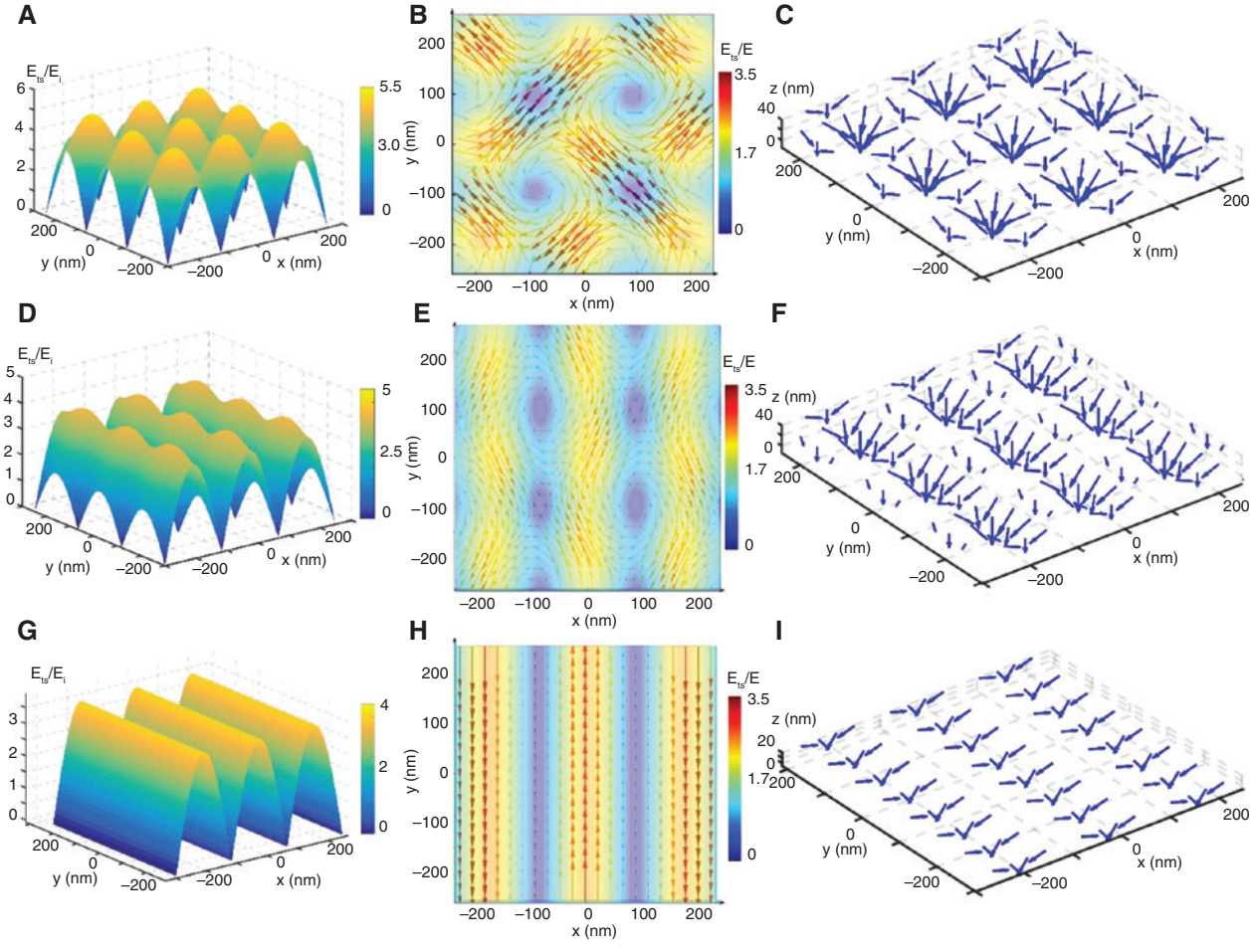

Figure 3: Electric field amplitude ratio, field vector distribution on the intensity background, and 3D distribution of optical gradient force acting on the colloidal silver NPs (radius $a = 10$ nm) in the orthogonal LSEW fields with different optical power intensity tuning factors. (A–C) $\gamma = 1$, (D–F) $\gamma = \sqrt{2}/2$, and (G–I) $\gamma = 0$.

case of $\gamma=\sqrt{2}/2$ shown in Figure 3D,E, the electric fields and optical gradient force fields show anisotropic in-plane distribution. As the orthogonal LSEW approaches a 1D configuration ($\gamma=0$), the electric fields, the distribution of electric fields, and the optical gradient force fields are shown in Figure 3G–I. With the exertion of the various configurations of optical forces presented above, the NPs are directed and aggregated toward the hot-spot areas, which leads to diverse shapes of ordered nano-patterned colloidal metasurfaces.

3 Conclusion

We have proposed a light-controlled rapid fabrication procedure of PFGP, which can produce large-area nano-patterned colloidal silver metasurfaces, using a low fluence irradiation of orthogonal LSEW within several minutes. The pattern orientation, nano-mound size, height, and spacing can be tuned as desired, by varying the intensity ratio of the incident laser beams, which provides a multidimensional parameter space to manipulate the nano-patterned metasurfaces. We have unveiled that the key contribution to the PFGP of nano-patterned colloidal metasurfaces arises from the cooperative exertion of optical forces on colloidal NPs in orthogonal LSEW fields. The morphology-correlated p-SERS characterizations and the numerical simulations further substantiate the interpretation of dynamical driving and binding processes of PFGP, which confirm the binding and polarization-stabilizing behavior of the NPs during the formation of nano-patterned metasurfaces. Such understanding of controllable dipolar coupling in the nano-patterned array by the nanostructured optical fields provides an important foundation for designing reconfigurable metasurfaces to manipulate light field polarizations at the nanoscale. It constitutes the fundamental step for the fabrication of complex functional nanostructures based on assembled NPs, which provides a new way for optical patterning and offers new perspectives on the rapidly emerging area of nano-photonics.

4 Materials and methods

4.1 Materials and sample fabrication

The spherical silver NP colloids were prepared by the widely used photochemical reduction method [28], which is a relatively simple and easy method for the fabrication of uniform colloidal silver NPs. $AgNO_3$ was dissolved in purified water and mixed with citrate in a 1:1 ratio (initial concentration, 1 mM). The solution was illuminated with ultraviolet light ($\lambda=350$ nm, $P=20$ mW) for 2 h. Thus, the aqueous solution containing Ag ions and a reducing agent results in the growth of the silver NPs through photochemical reduction. By using transmission electronic microscopy characterization, the silver colloid NPs are uniform, roughly spherical, and the average size is about 20 nm.

A quad-frustum prism (high refractive index glass n_1 of 1.90 at 532 nm; side length of the top square face: 3 cm; thickness: 1 cm; angle between the top and side faces: 50°) enclosed with a glass spacer (thickness ~0.50 mm) and a coverslip (thickness ~0.20 mm) is used as the PFGP cell. The silver colloids dispersed in purified water (refractive index n_2: 1.33; NP diameter: ~20 nm) were placed in the deposition cell and covered by a coverslip (thickness ~0.20 mm). Finally, the ordered nano-patterns were formed on the top surface of the prism by the exertion of the orthogonal LSEW fields constructed with four s-polarized synchronous laser beams from a single longitudinal mode (SLM) laser [SLM diode pump solid state (DPSS) laser, diameter ~ 5 mm, wavelength 532 nm, output power 250 mW; Elforlight Co. Ltd., UK] for several minutes. The original samples were rinsed with purified water and then dried with slight blow of high-purity N_2 gas (99.99%) for several minutes for further characterization.

4.2 Sample characterizations

The fabricated colloidal silver nano-patterns were characterized using a field-emission scanning electron microscope (FE-SEM, HITACHI, SU8010, Japan). The polarization nature of the grating patterns was studied via p-SERS spectroscopy. The p-SERS spectra of a 10 μl of 10 mM rhodamine 6G (99%, Aladdin, Shanghai, China) solution in isopropyl alcohol adsorbed on the colloidal silver nano-patterns were observed at different polarization directions of incident light with a confocal Raman microscope (alpha300R, WITec GmbH. Ltd, Germany). All spectra were detected by excitation with a linearly polarized incident laser (laser wavelength, 532 nm; laser power, ~1 mW; laser focal diameter, ~2 μm; accumulation time, 10 s on the sample). The angle ϕ is taken as the difference between the polarization direction of the incident excitation laser and one array direction, which can be varied by rotating the sample horizontally.

4.3 Numerical simulations and calculations

To obtain further insight into the polarization and dipolar interaction of colloidal silver NPs as employed in the PFGP experiments, the electric field distribution around the NPs in s-polarized orthogonal LSEW was simulated by a 3D finite-difference time-domain (FDTD) method. All simulation parameters were chosen to match the experimental conditions. The four s-polarized plane wave input laser beams were used to construct the orthogonal LSEW in the FDTD simulation. A real relative dielectric constant ε_m ($\varepsilon_m = n^2 = 1.77$) is considered for water, and the relative permittivity for silver NP is $\varepsilon_p = -9.15 + 0.81j$ in the LSEW field for $\lambda = 532$ nm. One layer of silver NPs is distributed as a square array with a spacing of 20 nm in the orthogonal LSEW fields. The diameter of the spherical NP is 20 nm, and the grid size is uniform with 1 nm. The vectorized Matlab code is written for the calculation of the optical forces exerted on the silver NPs in the orthogonal LSEW fields.

Acknowledgments: This work was partially supported by the National Natural Science Foundation of China (Funder Id: http://dx.doi.org/10.13039/501100001809, 11874102, 11474048, and 11274058). The authors gratefully acknowledge Prof. H.G. Duan for assistance with measurements of p-SERS spectra. The authors also appreciate the helpful discussions with Prof. M. Wang, Q.Y. Xu, and X.L. Liang.

Author Contributions

X. Huang initiated the research, conceived the experiments, analyzed the data, and wrote the manuscript. Y. Yang analyzed the data and assisted in manuscript preparation. K. Chen fabricated the arrays, and M. Qi measured the Raman spectra. Y. Li and P. Zhang carried out the optical simulations. S. Winnerl, H. Schneider, and Shuang Zhang assisted in manuscript preparation. All authors discussed the progress of research and reviewed the manuscript.

References

[1] Zheng GX, Mühlenbernd H, Kenney M, Li GX, Zentgraf T, Zhang S. Metasurface holograms reaching 80% efficiency. Nat Nanotech 2015;10:308–12.
[2] Khorasaninejad M, Chen WT, Devlin RC, Oh J, Zhu AY, Capasso F. Metalenses at visible wavelengths: diffraction-limited focusing and subwavelength resolution imaging. Science 2016;352:1190–4.
[3] Wang SM, Wu PC, Su VC, et al. Broadband achromatic optical metasurface devices. Nat Commun 2017;8:187.
[4] Kildishev AV, Boltasseva A, Shalaev VM. Planar photonics with metasurfaces. Science 2013;339:1232009.
[5] Yu NF, Genevet P, Kats MA, et al. Light propagation with phase discontinuities: generalized laws of reflection and refraction. Science 2011;334:333–7.
[6] Meinzer N, Barnes WL, Hooper IR. Plasmonic meta-atoms and metasurfaces. Nat Photon 2014;8:889–98.
[7] Yu NF, Capasso F. Flat optics with designer metasurfaces. Nat Mater 2014;13:139–50.
[8] Chen HT, Taylor AJ, Yu NF. A review of metasurfaces: physics and applications. Rep Prog Phys 2016;79:076401.
[9] Liu LX, Zhang XQ, Kenney M, et al. Broadband metasurfaces with simultaneous control of phase and amplitude. Adv Mater 2014;26:5031–6.
[10] Arbabi A, Horie Y, Bagheri M, Faraon A. Dielectric metasurfaces for complete control of phase and polarization with subwavelength spatial resolution and high transmission. Nat Nano 2015;10:937–43.
[11] Moreau A, Ciracì C, Mock JJ, et al. Controlled-reflectance surfaces with film-coupled colloidal nanoantennas. Nature 2012;492:86–9.
[12] Rozin MJ, Rosen DA, Dill TJ, Tao AR. Colloidal metasurfaces displaying near-ideal and tunable light absorbance in the infrared. Nat Commun 2015;6:7325.
[13] Alselrod GM, Huang JN, Hoang TB, et al. Large-area metasurface perfect absorbers from visible to near-infrared. Adv Mater 2015;27:8028–34.
[14] Siddique RH, Mertens J, Hölscher H, Vignolini S. Scalable and controlled self-assembly of aluminum-based random plasmonic metasurfaces. Light Sci Appl 2017;6:e17015.
[15] Gargiulo JL, Brick T, Violi IL, et al. Understanding and reducing photothermal forces for the fabrication of Au nanoparticle dimers by optical printing. Nano Lett 2017;17:5747–55.
[16] Nan F, Yan ZJ. Probing spatiotemporal stability of optical matter by polarization modulation. Nano Lett 2018;18:1396–401.
[17] Wang H, Levin CS, Halas NJ. Nanosphere arrays with controlled sub-10-nm gaps as surface-enhanced Raman spectroscopy substrates. Nano Lett J Am Chem Soc 2005;127:14992–3.
[18] Ashkin A. Acceleration and trapping of particles by radiation pressure. Phys Rev Lett 1970;24:156–9.
[19] Ashkin A, Dziedzic JM, Bjorkholm JE. Chu S. Observation of a single-beam gradient force optical trap for dielectric particles. Opt Lett 1986;11:288–90.
[20] Juan ML, Righini M, Quidant R. Plasmon nano-optical tweezers. Nat Photonics 2011;5:349–56.
[21] Gao DL, Ding WQ, Vesperinas MN, et al. Optical manipulation from the microscale to the nanoscale: fundamentals, advances and prospects. Light Sci Appl 2017;6:e17039.
[22] Kim JY, Kim H, Kim BH, et al. Highly tunable refractive index visible-light metasurface from block copolymer self-assembly. Nat Commun 2016;7:12911.
[23] Stewart SW, Akselrod GM, Smith DR, Mikkelsen MH. Toward multispectral imaging with colloidal metasurface pixels. Adv Mater 2016;29:1602971.
[24] Brzobohatý O, Karásek V, Šiler M, Chvátal L, Čižmár T, Zemánek P. Experimental demonstration of optical transport, sorting and self-arrangement using a 'tractor beam'. Nat Photon 2013;7:123–7.

[25] Chvátal L, Brzobohatý O, Zemánek P. Binding of a pair of Au nanoparticles in a wide Gaussian standing wave. Opt Rev 2015;22:157–61.
[26] Dholakia K, Zemánek P. Gripped by light: optical binding. Rev Mod Phys 2010;82:1767.
[27] Kawalec T, Józefowski L, Fiutowski J, Kasprowicz MJ, Dohnalik T. Spectroscopic measurements of the evanescent wave polarization state. Opt Commun 2007;274:341–6.
[28] Huang XP, Chen K, Qi MX, et al. Nanostructured grating patterns over a large area fabricated by optically directed assembly. Nanoscale 2016;8:13342–51.
[29] Fornel F. Evanescent waves: from Newtonian optics to atomic optics. Springer-Verlag, Berlin, 2000; pp. 5–8.
[30] Lim DK, Jeon KS, Kim HM, Nam JM, Suh YD. Nanogap-engineerable Raman-active nanodumbbells for single-molecule detection. Nat Mater 2010;9:60–7.
[31] Tumkur T, Yang X, Zhang C, et al. Wavelength-dependent optical force imaging of bimetallic Al-Au heterodimers. Nano Lett 2018;18:2040–6.
[32] Albaladejo S, Marques ML, Scheffold F, Saenz J. Giant enhanced diffusion of gold nanoparticles in optical vortex fields. Nano Lett 2009;9:3527–31.
[33] Albaladejo S, Marqués MI, Laroche M, Sáenz JJ. Scattering forces from the curl of the spin angular momentum of a light field. Phys Rev Lett 2009;102:113602.
[34] Min CJ, Shen Z, Shen JF, et al. Focused plasmonic trapping of metallic particles. Nat Commun 2013;4:2891.

Supplementary Material: The online version of this article offers supplementary material (https://doi.org/10.1515/nanoph-2018-0211).